Hybrid grating reflector with high reflectivity and broad bandwidth

Taghizadeh, Alireza; Park, Gyeong Cheol; Mørk, Jesper; Chung, Il-Sug

Published in:
Optics Express

Link to article, DOI:
10.1364/OE.22.021175

Publication date:
2014

Document Version
Publisher's PDF, also known as Version of record

Hybrid grating reflector with high reflectivity and broad bandwidth

Alireza Taghizadeh, Gyeong Cheol Park, Jesper Mørk, and Il-Sug Chung*

Department of Photonics Engineering (DTU Fotonik), Technical University of Denmark, DK-2800 Kgs. Lyngby, Denmark

**ilch@fotonik.dtu.dk*

Abstract: We suggest a new type of grating reflector denoted hybrid grating (HG) which shows large reflectivity in a broad wavelength range and has a structure suitable for realizing a vertical cavity laser with ultra-small modal volume. The properties of the grating reflector are investigated numerically and explained. The HG consists of an un-patterned III-V layer and a Si grating. The III-V layer has a thickness comparable to the grating layer, introduces more guided mode resonances and significantly increases the bandwidth of the reflector compared to the well-known high-index-contrast grating (HCG). By using an active III-V layer, a laser can be realized where the gain region is integrated into the mirror itself.

OCIS codes: (050.2770) Gratings; (140.7090) Ultrafast lasers; (230.4040) Mirrors; (050.6624) Subwavelength structures; (230.5298) Photonic crystals.

References and links

1. C. F. R. Mateus, M. C. Y. Huang, Y. Deng, A. R. Neureuther, and C. J. Chang-Hasnain, "Ultrabroadband mirror using low-index cladded subwavelength grating," IEEE Photon. Technol. Lett. **16**(2), 518–520 (2004).
2. C. F. R. Mateus, M. C. Y. Huang, L. Chen, and C. J. Chang-Hasnain, "Broad-band mirror (1.12-1.62 μm) using a subwavelength grating," IEEE Photon. Technol. Lett. **16**(7), 1676–1678 (2004).
3. M. C.Y. Huang, Y. Zhou, and C. J. Chang-Hasnain, "A surface-emitting laser incorporating a high index-contrast subwavelength grating," Nat. Photonics **1**(2), 119–122 (2007).
4. S. Boutami, B. Benbakir, J. L. Leclercq, and P. Viktorovitch, "Compact and polarization controlled 1.55 μm vertical-cavity surface-emitting laser using single-layer photonic crystal mirror," Appl. Phys. Lett. **91**, 071105 (2007).
5. M. C.Y. Huang, Y. Zhou, and Connie J. Chang-Hasnain, "Nano electro-mechanical optoelectronic tunable VCSEL," Opt. Express **15**, 1222 (2007).
6. I.-S. Chung, V. Iakovlev, A. Sirbu, A. Mereuta, A. Caliman, E. Kapon, and J. Mørk, "Broadband MEMS-tunable high-index-contrast subwavelength grating long-wavelength VCSEL," IEEE J. Quantum Electron. **46**(9), 1245–1253 (2010).
7. I.-S. Chung, J. Mørk, P. Gilet, and A. Chelnokov, "Subwavelength grating-mirror VCSEL with a thin oxide gap," IEEE Photon. Technol. Lett. **20**(2), 105–107 (2008).
8. I.-S. Chung and J. Mørk, "Silicon-photonics light source realized by III-V/Si-grating-mirror laser," Appl. Phys. Lett. **97**(15), 151–153 (2010).
9. C. Sciancalepore, B. B. Bakir, X. Letartre, J. Harduin, N. Olivier, C. Seassal, J. Fedeli, and P. Viktorovitch, "CMOS-compatible ultra-compact 1.55 μm emitting VCSELs using double photonic crystal mirrors," IEEE Photon. Technol. Lett. **24**(6), 455–457 (2012).
10. D. Fattal, J. Li, Z. Peng, M. Fiorentino, and R. G. Beausoleil, "Flat dielectric grating reflectors with focusing abilities," Nat. Photonics **4**(7), 466–470 (2010).
11. L. Carletti, R. Malureanu, J. Mørk, and I.-S. Chung, "High-index-contrast grating reflector with beam steering ability for the transmitted beam," Opt. Express **19**(23), 23567 (2011).
12. R. Magnusson, and M. Shokooh-Saremi, "Physical basis for wideband resonant reflectors," Opt. Express **16**(5), 3456–3462 (2008).

#214437 - $15.00 USD Received 17 Jul 2014; revised 15 Aug 2014; accepted 15 Aug 2014; published 25 Aug 2014

13. D. Rosenblatt, A. Sharon and A. A. Friesem, "Resonant grating waveguide structures," IEEE J. Quantum Electron. **33**(11), 2038–2059 (1997).
14. Y. Ding and R. Magnusson, "Resonant leaky-mode spectral-band engineering and device applications," Opt. Express **12**(23), 5661–5674 (2004).
15. P. Lalanne, J. P. Hugonin, and P. Chavel, "Optical properties of deep lamellar gratings: a coupled Bloch-mode insight," J. Lightwave Technol. **24**(6), 2442–2449 (2006).
16. V. Karagodsky and C. J. Chang-Hasnain, "Physics of near-wavelength high contrast gratings," Opt. Express **20**(10), 10888–10895 (2012).
17. M. G. Moharam, D. A. Pommet, E. B. Grann, and T. K. Gaylord, "Stable implementation of the rigorous coupled-wave analysis for surface-relief gratings: Enhanced transmittance matrix approach," J. Opt. Soc. Am. A **12**(5), 1077–1086 (1995).
18. G. Granet, B. Guizal, "Efficient implementation of the coupled-wave method for metallic lamellar gratings in TM polarization," J. Opt. Soc. Am. A **13**(5), 1019–1023 (1996).
19. L. Li, "Formulation and comparison of two recursive matrix algorithms for modeling layered diffraction gratings," J. Opt. Soc. Am. A **13**(5), 1024–1035 (1996).
20. E. Silberstein, P. Lalanne, J. P. Hugonin, and Q. Cao, "Use of grating theories in integrated optics," J. Opt. Soc. Am. A **18**(11), 2865–2875 (2001).
21. T. Estruch, F. Pardo, B. Portier, J. Jaeck, S. Derelle and R. Haidar, "Masons rule and Signal Flow Graphs applied to subwavelength resonant structures," Opt. Express **20**(24), 27155–27162 (2012).

1. Introduction

Recently, high-index-contrast gratings (HCGs) also known as photonic crystal mirrors (PCMs) have received increased attention due to their special characteristics. Among them, the capability of providing high reflectivity over a broad wavelength range makes the HCG an attractive alternative to distributed Bragg reflectors (DBRs) in vertical cavity devices, in particular in vertical-cavity surface-emitting lasers (VCSELs). The reflectivity of an HCG with several hundred nanometers thickness is as high as that of a DBR with thickness of several micrometers [1, 2]. Huang et al. [3] and Boutami et al. [4] independently demonstrated VCSELs with a HCG as a reflector. Since then, various novel vertical-cavity laser structures employing the HCG have been reported, demonstrating MEMS-based wavelength tunability [5, 6], strong single-transverse-mode operation [7], and integration with an SOI wafer [8, 9]. Another interesting feature that might be integrated to VCSELs is the possibility of beam steering or focusing [10, 11]. So far, there has been significant theoretical efforts to explain the mechanism responsible for the broadband nature of reflectivity spectrum. These can be separated into two groups: one based on in-plane leaky modes above light line [12–14] and the other based on vertically-propagating Bloch modes [15, 16]. A requisite common to all the literature is that the grating should be surrounded by low refractive index materials, as shown in Fig. 1(a), so as to provide broad bandwidth, e.g., larger than 100 nm.

In this paper, we suggest a new grating reflector structure that does not rely on this requisite. As shown in Fig. 1(b), the new structure, denoted hybrid grating (HG), consists of a grating layer and a high-refractive-index cap layer. The cap layer can be even thicker than the grating layer. In the context of second-order diffraction gratings, waveguides with shallow gratings are known to exhibit a narrow-band high reflectivity [13], but no structure with deep grating has been reported for broadband high reflectivity. The suggested HG has several interesting properties. The HG can provide high reflectivity over a larger bandwidth compared to the HCG. The reflection process in the HG is discussed using two conceptually different approaches, i.e., the leaky mode picture and the Bloch mode picture. The incident angle dependence of reflectivity, penetration depth, and fabrication tolerance are investigated as well. Furthermore, possibility of the cap layer including an active material like quantum wells (QWs) or quantum dots (QDs), enable new and very compact laser and photodetector designs. The expected benefits of such device designs are discussed.

#214437 - $15.00 USD Received 17 Jul 2014; revised 15 Aug 2014; accepted 15 Aug 2014; published 25 Aug 2014

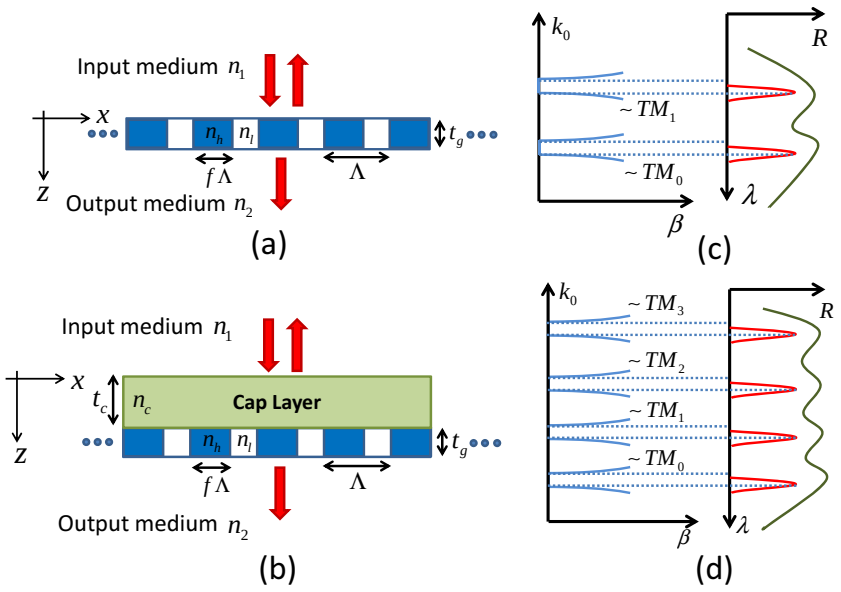

Fig. 1. (a) and (b) show schematic cross-sectional views of an HCG and an HG, respectively. In both cases a plane wave is incident from the top in the surface normal direction and similar results can be obtained for incident light from bottom. n_i and t_i represent refractive index and thickness of each part, respectively. Λ and f denote the periodicity and duty cycle of the grating. (c) and (d) are dispersions of leaky modes (blue curves) and reflectivity spectra (green curves) for the HCG and the HG, respectively. $k_0 = 2\pi/\lambda_0$, and β is the real part of propagation constant of a leaky mode. The red curves show the appeared resonance due to individual GMRs which will overlap to make the total reflectivity spectra (green curves)

2. Simulation method and results

We have developed an in-house three-dimensional (3D) vectorial simulator based on rigorous coupled wave analysis (RCWA) method [17–20]. Our simulator can handle absorbing boundary conditions for simulation of finite structures as well as periodic boundary conditions. For the studies in this paper, a two-dimensional (2D) simulation setup with periodic boundary condition in x direction is used to obtain reflectivity spectra and field profiles. For simplicity, it is assumed that the materials are lossless and non-dispersive, which is a good approximation in the wavelength range of our interest. In this method, firstly the Bloch modes of each layer propagating along the z direction are calculated by solving an eigenvalue problem based on Fourier expansion of the fields and permittivity [17, 18]. Then, the field in each layer is expressed as a summation of these Bloch modes with unknown coefficients. Involving boundary conditions at layer interfaces and the scattering matrix method (SMM) [19], the unknown coefficients are determined. In all our simulations, transverse magnetic (TM) polarized light, i.e., electric field perpendicular to the grating bars is considered. Analogously, one may design a broadband reflector for transverse electric (TE) polarized light by changing structure dimensions.

Schematic cross-sectional views of an HCG and an HG are shown in Figs. 1(a) and 1(b), respectively. To investigate the effect of the cap layer in the HG, the same grating parameters are used for HG and HCG. The parameter values used in the simulation are given in the caption of Fig. 2. Since the grating parameters are chosen to provide a flat high-reflectivity plateau for the HCG, the HG structure may not give a perfectly flat reflectivity plateau. As noticed in

#214437 - $15.00 USD Received 17 Jul 2014; revised 15 Aug 2014; accepted 15 Aug 2014; published 25 Aug 2014

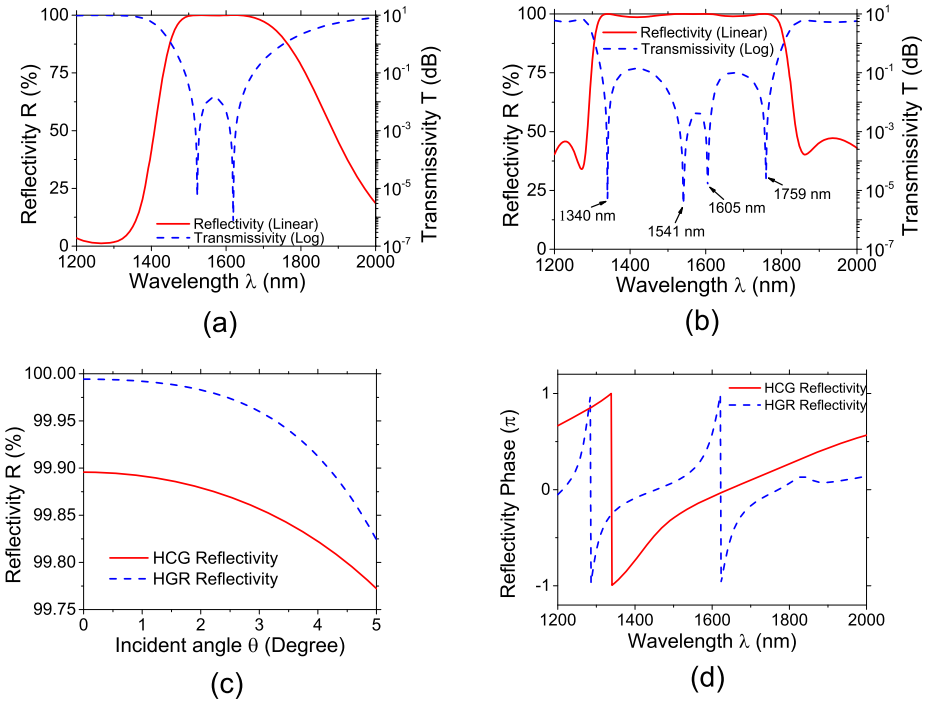

Fig. 2. Reflectivity and transmissivity spectra of (a) conventional HCG and (b) HG. Grating parameters common for HCG and HG are Λ=720 nm, t_g=497 nm, f=45 %, n_h=3.48, n_l=1.0, n_1=1.0, and n_2=1.0. Cap layer parameters for HG are t_c=370 nm and n_c=3.166. Parameter symbols are defined in Fig. 1. (c) Incident angle dependence of reflectivity at 1550-nm wavelength for HCG and HG. (d) Reflectivity phase spectra for HCG and HG.

'hybrid', the cap layer in the HG can be made of a different material than the grating: In the considered HG, an InP cap layer on a Si grating layer is assumed.

Reflectivity and transmissivity spectra of the designed HCG and HG are shown in Figs. 2(a), and 2(b), respectively. The dips in the transmissiviy spectra correspond to the guided mode resonances (GMRs) [14]. It can be observed that there are two GMRs in the high reflection bandwidth of the HCG while there are four GMRs in the HG case which result in a high reflectivity over significantly larger bandwidth compared to the HCG. For this example, $\Delta\lambda/\lambda_0 \approx 12\%$ in the HCG structure, while $\Delta\lambda/\lambda_0 \approx 30\%$ in the HG structure, where $\Delta\lambda$ is wavelength range with reflectivity higher than 99% and λ_0 is 1550 nm. As shown in Fig. 2(c), the HG has similar incident angle dependence of reflectivity as the HCG, at the center of stop band, i.e., 1550-nm wavelength. Furthermore, at the 1550-nm wavelength, the HG has a similar phase slope as the HCG, which means both have a similar phase penetration depth [6]. Around 1620-nm wavelength, there exists another penetration depth in HG. It is expected that the angle dependence and phase spectra of the HG should be able to be engineered as in the HCG case.

The HG reflector has good tolerance to fabrication errors. During fabrication steps including epitaxy growth, cap layer thickness, t_c, grating thickness, t_g, and grating width, $f\Lambda$ may have $\pm$ 10 nm variations from designed values. Grating period, Λ can be relatively accurately defined. To estimate the effect of fabrication variations in t_c, t_g, and $f\Lambda$ on reflectivity, Monte Carlo

#214437 - $15.00 USD Received 17 Jul 2014; revised 15 Aug 2014; accepted 15 Aug 2014; published 25 Aug 2014

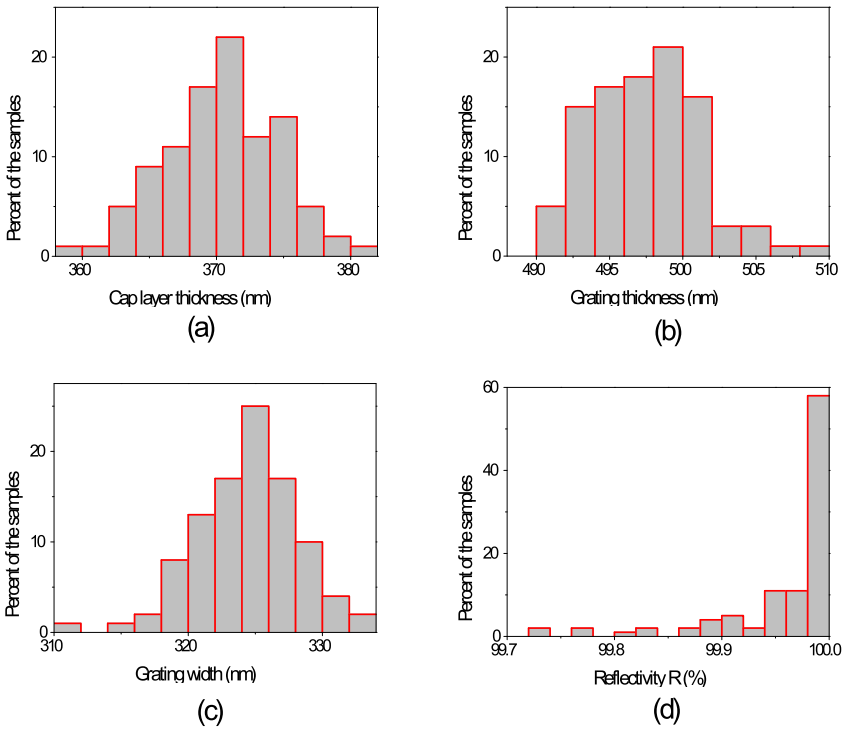

Fig. 3. Fabrication tolerance analysis with 100 samples. Histogram distributions of (a) cap layer thickness, (b) grating thickness, and (c) grating bar width. (d) Monte Carlo analysis result for reflectivity.

analysis is performed. In this analysis, 100 samples each with different t_c, t_g, and $f\Lambda$ values are chosen. Each parameter value is chosen to un-correlated to each other and to have a normal distribution with a probability density function of $f(x) = \frac{1}{\sigma\sqrt{2\pi}} \exp(-\frac{x-x_0}{2\sigma^2})$ where x_0 is the value of designed parameter and 3σ is the fabrication error. We have assumed $\sigma = 4$ nm which corresponds to ± 12 nm error. Figures 3(a), 3(b), and 3(c) show the histogram distribution of each parameter in the 100 samples chosen. Monte Carlo analysis result presented in Fig. 3(d) shows that all HG samples have reflectivity above 99.7%, indicating the HG is tolerable to most of probable fabrication errors.

If light is incident from the grating side, i.e., the bottom side in this example, the reflectivity spectrum is the same as in Fig. 2(b) while the reflection phase spectrum becomes different.

3. Analysis of reflection mechanism

3.1. Leaky mode picture

In the leaky mode picture, the HCG is viewed as a slab waveguide with a periodic index modulation, also denoted as photonic crystal slab [12]. The broadband nature of the reflectivity is understood as a result of GMRs between leaky band-edge modes of the grating slab and free-space modes outside the grating slab. The band-edge modes are leaky since they are above the light line in the band dispersion diagram. These GMRs can be viewed as Fano resonances between the discrete grating modes and the continuous free-space modes. As illustrated in Fig.

#214437 - $15.00 USD Received 17 Jul 2014; revised 15 Aug 2014; accepted 15 Aug 2014; published 25 Aug 2014

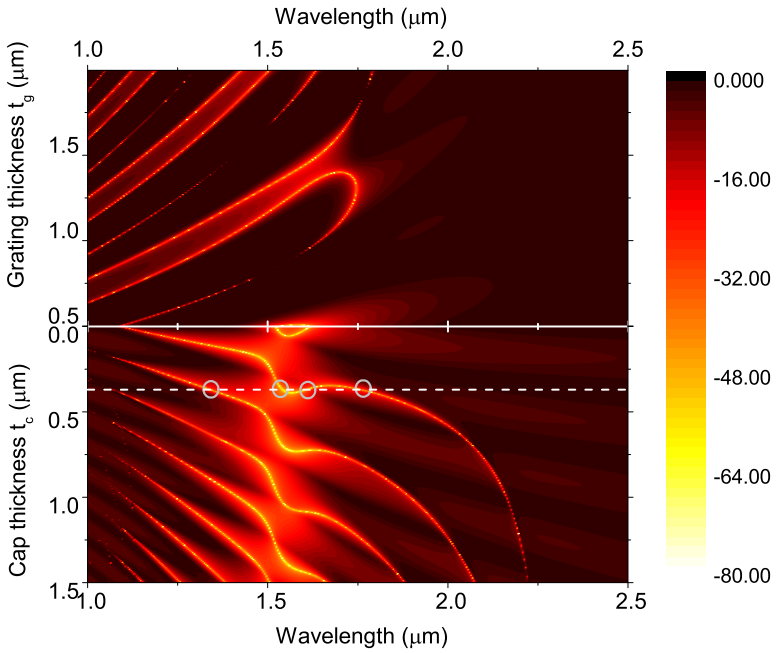

Fig. 4. Contour plot of transmissivity in dB as a function of wavelength, grating thickness, t_g, and cap layer thickness, t_c. In the upper graph, t_g is increased from 0.497 μm to 1.997 μm while t_c is zero. In the lower graph, t_c is increased from 0 to 1.5 μm while t_g is kept to 0.497 μm. The white dashed line shows the cap layer thickness of the HG structure considered in Fig. 2 and the circles indicate the wavelengths of the four GMRs.

1(c), HCGs have typically two GMRs, each from the two slab waveguide modes TM_0 and TM_1. The reason why only one of two band-edge modes in TM_0 (or TM_1) gives rise to GMR is that in the other band-edge mode, two counter-propagating modes of the grating slab cancel each other [12]. By increasing the thickness of the HCG, as known from waveguide theory more modes will be introduced.

Figure 4 shows a simulated transmissivity contour as a function of wavelength, grating layer thickness, and cap layer thickness. Here, bright lines correspond to GMRs, i.e., excited band-edge modes. In the HCG case (upper graph), as we expect, more modes are introduced as the grating layer thickness is increased. The same trend is observed for the HG case (lower graph) as the cap layer thickness is increased while the grating layer thickness is fixed. A difference between the HG and the HCG structure is that for the HG structure good overlaps between different modes can be provided due to cap layer: In the HCG structure, only two nearby band-edge modes overlap while others are well separated. As a result, a broader high-reflectivity is obtained in the HG case than in the HCG case.

The field amplitude of the 0-th harmonic in the cap layer is comparable to or higher than that in the incident medium, i.e., air in the current example. Figure 5 shows decomposed harmonics at the four GMR wavelengths indicated in Fig. 2. All propagating modes have almost all their power in harmonics up to the second order. The round-trip optical path lengths of the 0-th harmonics within the cap and grating layers can be found using the effective refractive indices

#214437 - $15.00 USD Received 17 Jul 2014; revised 15 Aug 2014; accepted 15 Aug 2014; published 25 Aug 2014

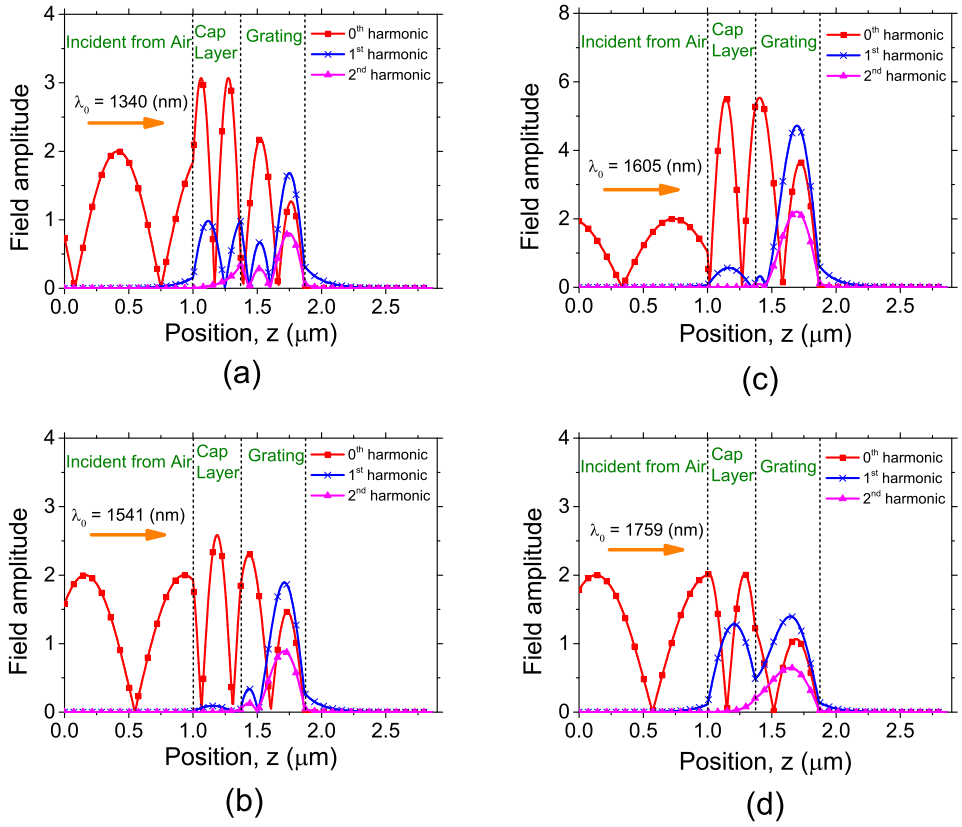

Fig. 5. Magnetic field amplitude profiles in the HG, decomposed into 0-th (red), 1-st(blue), and 2-nd(magenta) harmonics at different GMR wavelengths, λ: (a) λ=1340 nm. (b) λ=1541 nm. (c) λ=1605 nm. (d) λ=1759 nm. Incident light is assumed to be from the left.

of the layers multiplied by their thicknesses. They are approximately 2.5λ, 3.2λ, 3.5λ, and 3.7λ at λ=1759 nm, 1605 nm, 1541 nm, and 1340 nm, respectively. Note that at λ=1605 nm and 1340 nm, the amplitudes of the 0-th harmonics are higher in the cap layer and grating than in the incident medium. At these wavelengths, the round-trip path lengths are close to an integer multiple of the wavelength, which result in weak accumulation of energy inside the cap layer and grating similar to a Fabry Pérot cavity. At the other wavelengths, the amplitude of the 0-th harmonic has comparable magnitude in the cap layer, grating and input medium.

3.2. Bloch mode picture

In the Bloch mode picture, the basis modes considered are the Bloch modes of a grating structure that is periodic in the *x* direction and infinite in the *y* direction [15]. Alternatively, this structure can be seen as a coupled waveguide array [16]. It has been shown that only those Bloch modes with a real propagation constant, β in *z* direction participate in the reflection process [15, 16]. For HCG structure, in the wavelength range of our interest, i.e., around 1550 nm, there are only two propagating Bloch modes in the grating. Outside the grating, there is one propagating free-space mode, i.e., the 0-th order harmonic. A signal flow graph (SFG) in Fig.

#214437 - $15.00 USD Received 17 Jul 2014; revised 15 Aug 2014; accepted 15 Aug 2014; published 25 Aug 2014

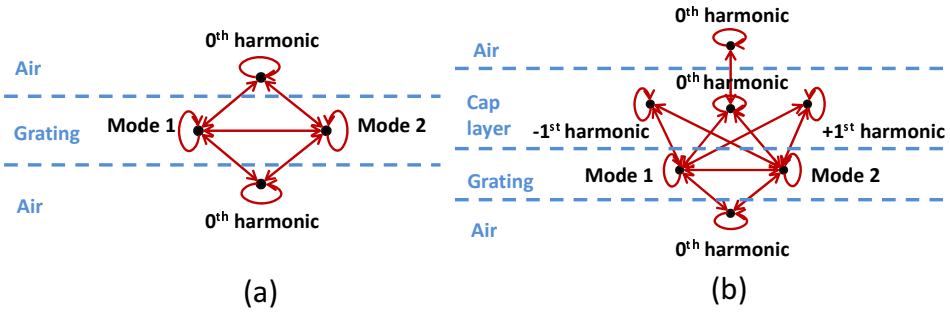

Fig. 6. SFGs of the propagating modes in each layer for (a) HCG and (b) HG structure. Black dots represent propagating modes at each layer. Red arrows denote the interactions between the modes which take place at interfaces. Circular arrows mean self coupling (reflectivity of a mode to itself) at interfaces.

6(a) illustrates how these modes interact with one another at interfaces [21]. The broadband reflection properties can be understood as the combined result of propagations of Bloch modes within the grating layer and their reflection at the interfaces. Each dot which is called a node correspond to a propagating mode. Interaction between modes are shown by arrows and called branches which take place at interfaces. The circular arrow represents reflection of a mode back to itself at the interface.

In the HG as well as in the HCG case, only propagating modes in the layers participate in the reflection process. As shown in Fig. 6(b), there are two propagating modes in the grating, several (three or five) propagating modes in the cap layer, and a propagating free-space mode outside the HG structure. In homogeneous layers e.g. cap layer each mode corresponds to a single spatial harmonic (or diffraction order) [17]. So in the input and output media, the only propagating mode corresponds to 0-th harmonic (0-th diffraction order) and for the cap layer due to the higher refractive index the three propagating modes correspond to 0-th and $\pm$1-st harmonics. Note that the $\pm$1-st harmonics interact with the two Bloch modes in the grating layer, but not with the 0-th harmonic in the air. Thus, it is expected that most of the power coupled from the Bloch modes in the grating layer to the $\pm$1-st harmonics is returned to the Bloch modes with some phase change, not escaping from the HG structure. From this arguing, it is qualitatively understandable that adding the cap layer introduces change in GMR wavelengths but not in peak reflectivity.

Considering only the propagating modes in the different layers, the reflectiviy spectrum of the HG can be reconstructed with a good approximation to rigorous RCWA result. Firstly, as illustrated in Fig. 7(a), all evanescent modes with an imaginary propagation constant are discarded in all layers. This simplifies the scattering matrices r_1 and r_2 at the interfaces and the propagation matrix $\exp(-j2\beta d)$. Using these simplified matrices, the reflectivity, r_{eq} from the HG can be found from a matrix version of the well-known reflectivity formula for two interfaces, as illustrated in Fig. 7(b).

$$r_{eq} = \frac{r_1 + r_2 \exp(-j2\beta d)}{1 + r_1 r_2 \exp(-j2\beta d)} \tag{1}$$

where 1 represents a unity matrix. In Fig. 7(c), the reflectivity spectrum obtained by this semi-analytic approach is compared with the rigorous RCWA result, showing a good agreement, especially in the high reflectivity region. This supports the explanation that high value of the reflectivity and its broadband nature depends mainly on propagating modes.

#214437 - $15.00 USD Received 17 Jul 2014; revised 15 Aug 2014; accepted 15 Aug 2014; published 25 Aug 2014

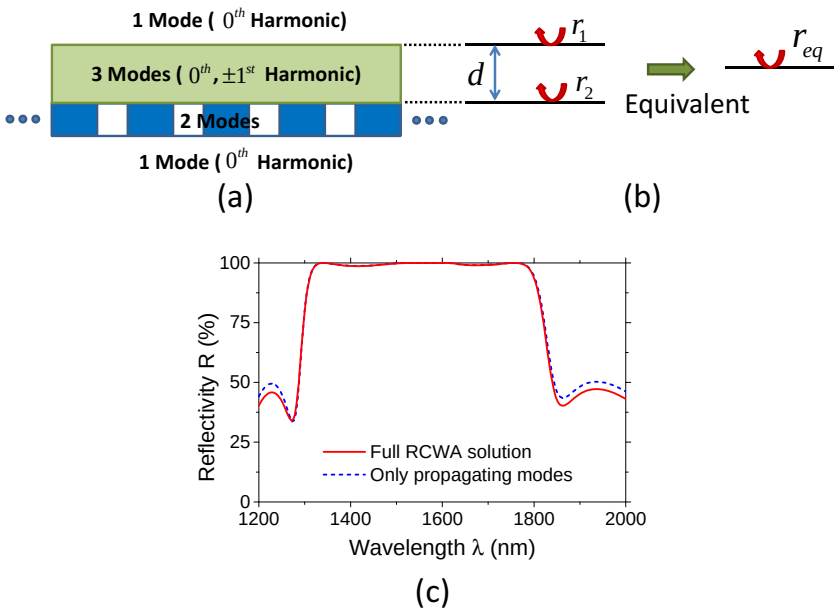

Fig. 7. (a) Schematic cross-sectional view of the HG with considered modes in each layer. (b) The equivalent reflectivity from the two interface of the cap layer and grating. (c) Calculated reflectivity spectrum of the structure shown in Fig. 2 using full RCWA (red solid line) and with discarding non-propagating modes (blue dashed line). It shows a very good agreement especially in the wavelength region with high reflectivity.

4. Potential for a new type of lasers and detectors

An interesting possibility with the HG is that the cap layer may include an active material such as QWs or QDs. Using this active HG, one may implement a new type of vertical-cavity laser structure where light is generated inside the mirror, rather than in the middle of a cavity. For example, the new laser structure may consists of a passive mirror, a very thin passive cavity, e.g., $\lambda/2$-air cavity, and an active HG reflector.

Compared to a conventional VCSEL structure, a laser structure employing an active HG can achieve much higher confinement factor since the vertical cavity length can be considerably shorter, thanks to the thin passive dummy cavity. Furthermore, the field amplitude enhancement at the anti-node in the cap layer as discussed in relation to Fig. 5 contributes to further increase of the confinement factor. This higher confinement factor, equivalently, smaller modal volume may lead to higher modulation speed.

5. Conclusion

We have suggested a novel HG that consists of a sub-wavelength grating layer and an unpatterned high-refractive-index cap layer. Numerical simulations show that the HG reflector has a near-unity reflectivity in a broad bandwidth, surpassing that of a conventional HCG. It has been revealed that the cap layer introduces more GMRs without loss of peak reflectivity leading to this broader high-reflectivity bandwidth. We have also shown that this broadband reflection properties originate mainly from propagating modes within the structure. Provided an active material is included as part of the cap layer, a VCSEL structure with an ultra-compact modal volume can be realized with a potential of very high modulation speed. Experimental demonstration of the HG reflector will be reported elsewhere soon.

#214437 - $15.00 USD Received 17 Jul 2014; revised 15 Aug 2014; accepted 15 Aug 2014; published 25 Aug 2014

Acknowledgments

This work has been supported by the Danish Research Council (Sagsnr. 11-106620) as well as Villum Fonden via the VKR Center of Excellence NATEC.

#214437 - $15.00 USD Received 17 Jul 2014; revised 15 Aug 2014; accepted 15 Aug 2014; published 25 Aug 2014